

# *Effect of the geometries of current collectors on the power density in a solid oxide fuel cell*

Peiwen Li<sup>\*1</sup>, Gege Tao<sup>2</sup>, Hong Liu<sup>3</sup>

<sup>1, 3</sup>Department of Aerospace and Mechanical Engineering, The University of Arizona, Tucson, AZ 85721, USA

<sup>2</sup>Materials and Systems Research, Inc. Salt Lake City, Utah, UT 84104, USA

Received Date: 26 Jul.; 2011

Accepted: 18 Aug.; 2011

## **ABSTRACT**

An analytical model is proposed and an analysis is conducted for solid oxide fuel cells with goals of higher power densities. The analytical model is designed to help optimize the size, spacing, and geometrical shapes of current collectors. The model fully considers the ohmic, species concentration, and activation polarizations. From the analysis of several cases, it is recommended that 3D pillars be used for the current collectors in SOFCs while incorporating appropriate measures to ensure a uniform flow distribution. It is also clear that unless limited by the fabrication technologies for the bipolar plates, smaller control areas and current collectors are preferable for SOFCs to have higher power densities.

## **Keywords**

SOFC, optimization, current collectors, bipolar plate, design .

## **1. Introduction**

High power density is very important for solid oxide fuel cells (SOFC) to be used as power sources in transportation tools such as trains, trucks, buses, and cars. It is obvious that high power density directly translates to a low cost of fuel cells per unit of power. It also allows for compact design leading to less space occupied by the fuel cell power unit.

There are several approaches to developing high power density solid oxide fuel cells. One very challenging but effective way for power density improvement is to lower the internal ohmic loss by using a high ion-conductive electrolyte.

Research work and progress on this direction has been reported in literature [1-5]. Significantly improved triple-phase-boundary length [6-9] of

electrochemical reaction is also very effective at lowering activation polarization, resulting in higher power density. Some recent works [10] focus on using the so-called functional graded layer in order to improve the triple-phase-boundary length.

Although it has not received great attention, optimized design of the current collectors and gas channels should not be underestimated as a means of improving the power density of solid oxide fuel cells.

Better gas mixing and uniform flow fields help reduce the resistance to mass transfer [11-12] and thus reduce the concentration polarization. Optimum distribution of the current collectors should make it possible to compromise between a short length of current collection and the

<sup>\*</sup>Corresponding author: Peiwen Li (email:peiwen@email.arizona.edu)  
Tel. +01-520-626-7789; Fax: +01-520-621-8191

maintenance of a sufficiently large active area for electrochemical reaction. Consequently, maximum power density should be obtained.

There are two aspects to consider when determining the best design of the gas delivery field and distribution of current collectors. The first is the geometry of the current collectors. The geometry of the current collectors decides for the structure of flow field for gas delivery and removal, greatly affecting the mass transfer performance. The second aspect is the optimization of the selected current collector distribution.

SOFCs are able to operate on reformed hydrocarbon fuel while producing carbon dioxide and water vapor as waste. In a planar-type SOFC, gas flow fields are configured on bipolar plates. The gas flow field may simply comprise of multiple flow channels in parallel or a serpentine channel. The channels in this configuration are basically formed by 2-dimensional ribs, as shown in Fig.1. From mass transfer point of view, this type of flow field design has the disadvantage of no communication between flows from different channels.

Using 3-dimensional ribs or pillars distributed in a flow field, as shown in Fig.2, is expected to have mass transfer enhancement and thus a better fuel cell performance [13, 14]. However, application of this concept to actual fuel cells has long been restricted by the fact that a uniform distribution of flow in such a flow field is difficult to enforce [15, 16]. Recently, a uniform flow distributor with very good performance was invented by the current authors'

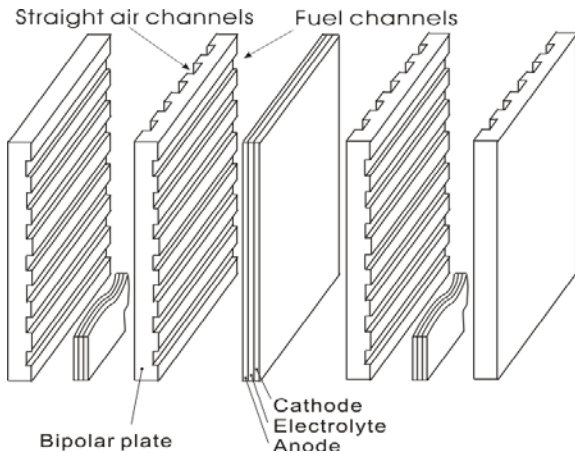


Fig.1: Two-dimensional current collectors on bipolar plates

group [17]. Therefore, assuming the use of this new flow distributor, 3D current collectors will be studied in this work. A comparison of the performance of the 3D current collector with that of 2D current collectors will be carried out.

## 2. Analysis and modeling

For convenience of analysis, one single current collector is to be considered. The collector is located at the center of a reaction area that can also be called the control area, as shown in Fig. 3 for both 2D and 3D cases. An electrical circuit representing the current conduction process will establish the relationship between the parameters, including the dimensions of current collectors, current and current density in the control area, the fuel cell operating temperature, properties of cell components, and the power density.

The electromotive force shown in the circuit network in Fig.3 is net voltage, the standard electromotive force reduced by both concentration polarization and activation polarization.

$$\bar{E} = E^o - \eta_{conc} - \eta_{act} \quad (1)$$

Solution for the network circuit will consequently find the potential difference ( $V_{cell}$ ) between the current collectors of the cathode and anode sides.

The activation polarization is given by the Butler-Volmer equation:

$$i = i_0 \left\{ \exp\left(\beta \frac{n_e F \eta_{act}}{RT}\right) - \exp\left[-(1-\beta) \frac{n_e F \eta_{act}}{RT}\right] \right\} \quad (2)$$

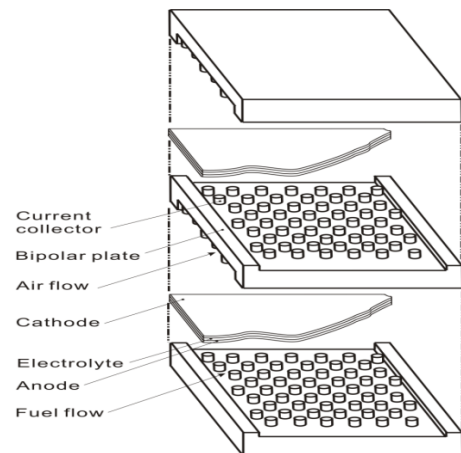


Fig.2: Three-dimensional current collectors on bipolar plates

Where  $\beta$  is the transfer coefficient, approximately 0.5;  $i$  is the actual current density through the active electrolyte layer in the fuel cell; and  $i_0$  is the exchange current density.  $n_e$  is the number of electrons transferred per mole of fuel in the electrochemical reaction. For a SOFC,  $n_e=2$ . Substituting values of  $\beta$  and  $n_e$  into Eq. (2) gives:

$$i = 2i_0 \sinh\left(\frac{F\eta_{act}}{RT}\right) \quad (3)$$

From which the activation polarization is consequently expressed as:

$$\eta_{act} = \frac{RT}{F} \ln \left[ \left( \frac{i}{2i_0} \right) + \sqrt{\left( \frac{i}{2i_0} \right)^2 + 1} \right] \quad (4)$$

In order to find the activation polarization using Eq. (4), the exchange current density  $i_0$  must be properly selected. From the electrochemistry point of view, the exchange current density of solid oxide fuel cells depends strongly on the triple-phase-boundary (TPB) length. The conventional fabrication technique of SOFCs makes a clear interface of the electrode and electrolyte layers, allowing an exchange current density of about 3000 A/m<sup>2</sup> for the cathode and 6000 A/m<sup>2</sup> for the anode.

Instead of a clear change in composition and micro-structure between the electrode and electrolyte materials, a functional graded layer made by modern fabrication techniques allows an overlap and mixing of electrode and electrolyte materials. This has been proven to improve the exchange current density on several occasions. The state-of-the-art planar type SOFC may have a power density of 1.8W/cm<sup>2</sup>, much greater than that of earlier stage SOFCs [9]. Performance comparisons of SOFCs with and without functional layers have found that the exchange current densities of 12000 A/m<sup>2</sup> and 24000 A/m<sup>2</sup> on cathode and anode respectively might be pertinent for those SOFCs with functional layers.

The concentration polarization is reflected by the second term in the following Nernst equation:

$$E = \frac{-\Delta G^o}{2F} + \frac{RT}{2F} \ln \frac{\left(\frac{P_{H_2}}{P^o}\right)\left(\frac{P_{O_2}}{P^o}\right)^{0.5}}{\left(\frac{P_{H_2O}}{P^o}\right)} \quad (5)$$

The concentration polarization causes a reduction of the electromotive force of a fuel cell; thus, the value of the second term in Eq. (5) is negative.

The partial pressures of the reactants and products at the anode-electrolyte and cathode-electrolyte interfaces are the parameters which determine the concentration polarization. Therefore, the mass transfer process has to be analyzed to find the mass concentration and partial pressures of each species.

The mass transfer resistances exist in the bulk flow, porous electrode, and porous graded functional layers (which are present in modern solid oxide fuel cells).

As a consequence of the mass transfer resistances, the partial pressures of reactants at the reaction site are lower than that in the bulk flow. Conversely, the partial pressures of products at the reaction site are higher than that in the bulk flow, as schematically shown in Fig. 4.

A zero-dimensional mass transfer model is applied to find the concentration polarization. As an example, consider the mass transfer of oxygen on the cathode side. For a SOFC with graded functional layers, the mass transfer of oxygen from bulk flow to the electrode/electrolyte interface experiences three processes: convective mass transfer, diffusion in the porous electrode layer, and diffusion in the functional layer.

$$\dot{m}_{O_2} = Ah_{O_2} (\rho_{\infty}^{O_2} - \rho_c^{O_2}) \quad (6)$$

$$\dot{m}_{O_2} = A \frac{\rho_c^{O_2} - \rho_{it}^{O_2}}{\frac{\delta_c}{D_{eff-c}} + \frac{\delta_{cfl}}{D_{eff-cfl}}} \quad (7)$$

Where the effective diffusivities for the porous cathode and cathode functional layers are  $D_{eff-c}$  and  $D_{eff-cfl}$ . These are functions of the gas diffusivity and porosity of the porous media:

$$D_{eff-c} = D_{O_2, N_2} \varepsilon_c^{1.5} \quad (8)$$

$$D_{eff-cfl} = D_{O_2, N_2} \varepsilon_{cfl}^{1.5} \quad (9)$$

The mass transfer rate which is proportional to the difference of the concentration in the bulk flow and at the cathode/electrolyte interface is then determined.

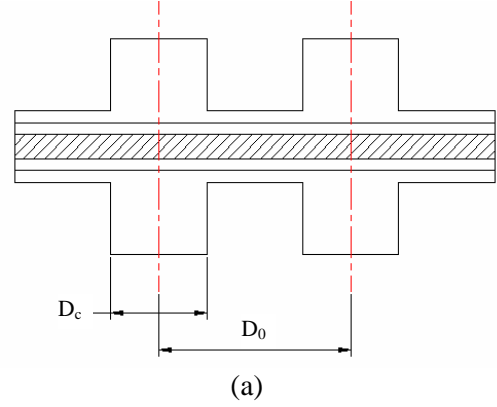
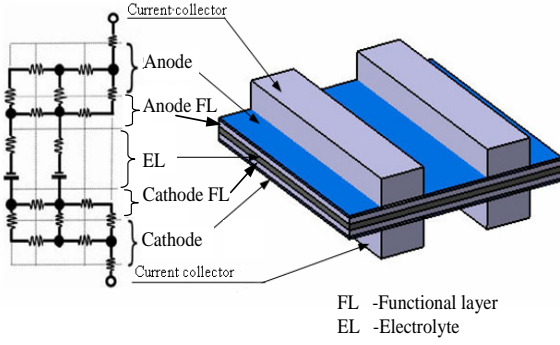


Fig. 3: Current collectors and circuits for current collection. (a) Model for two dimensional current collectors; (b) Model for three dimensional current collectors

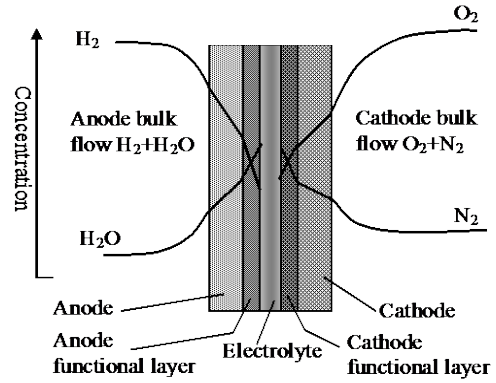


Fig. 4: Mass transfer processes in a SOFC

$$\dot{m}_{O_2} = A(\rho_{\infty}^{O_2} - \rho_{it}^{O_2}) \frac{1}{\frac{1}{h_{O_2}} + \frac{\delta_c}{D_{eff-c}} + \frac{\delta_{cfl}}{D_{eff-cfl}}} \quad (10)$$

$$\dot{m}_{O_2} = A(\rho_{\infty}^{O_2} - \rho_{it}^{O_2}) H_{O_2} \quad (11)$$

Where

$$H_{O_2} = \frac{1}{\frac{1}{h_{O_2}} + \frac{\delta_c}{D_{eff-c}} + \frac{\delta_{cfl}}{D_{eff-cfl}}} \quad (12)$$

The oxygen transferred to the reaction site is consumed for power generation. Thus the oxygen flow is related to the current output from the reaction area, controlled by the current collector under investigation:

$$\dot{m}_{O_2} = \frac{I}{4F} M_{O_2} \quad (13)$$

Substituting Eq. (13) into Eq. (11) yields an expression for the oxygen concentration at the cathode/electrolyte interface:

$$\frac{I}{4F} M_{O_2} = A H_{O_2} (\rho_{\infty}^{O_2} - \rho_{it}^{O_2}) \quad (14)$$

$$\rho_{it}^{O_2} = \rho_{\infty}^{O_2} - \frac{I}{4FAH_{O_2}} M_{O_2} \quad (15)$$

Where the mean oxygen concentration in the bulk flow may be approximated as:

$$\rho_{\infty}^{O_2} = \frac{\rho_{in}^{O_2} + \rho_{out}^{O_2}}{2} \quad (16)$$

Considering the inlet and outlet mass flow rate of the oxygen and the volumetric flow rate of the air stream, the concentrations of oxygen are:

$$\rho_{in}^{O_2} = \frac{\dot{m}_{in}^{O_2}}{\dot{V}_{O_2} + \dot{V}_{N_2}} \quad (17)$$

$$\rho_{out}^{O_2} = \frac{\dot{m}_{in}^{O_2} - \dot{m}_{O_2}}{\dot{V}_{N_2} + \dot{V}_{O_2} - \frac{\dot{m}_{in}^{O_2} - \dot{m}_{O_2}}{\rho_{in}^{O_2}}} \quad (18)$$

Given the mass transfer and electrolyte area,  $A$ , and the current density of the fuel cell  $i$ , the total current of the fuel cell becomes

$$I = iA \quad (19)$$

Substituting Eqs. (16)-(19) into Eq. (15), the oxygen concentration at the interface of the electrolyte/cathode is

$$\rho_{it}^{O_2} = \left( \frac{\dot{m}_{in}^{O_2}}{\dot{V}_{O_2} + \dot{V}_{N_2}} + \frac{\dot{m}_{in}^{O_2} - \frac{I}{4F} M_{O_2}}{\dot{V}_{N_2} + \dot{V}_{O_2} - \frac{\dot{m}_{in}^{O_2} - \frac{I}{4F} M_{O_2}}{\rho_{in}^{O_2}}} \right) / 2 - \frac{I}{4FAH_{O_2}} M_{O_2} \quad (20)$$

In order to obtain the partial pressure of oxygen, the concentration of nitrogen in the air flow is needed. In a similar analysis, the nitrogen concentration is obtained. From the mass transfer equation similar to Eq. (6), there is:

$$\rho_{\infty}^{N_2} = \rho_{it}^{N_2} \quad (21)$$

The average concentration of nitrogen in the bulk flow at the inlet and outlet are given respectively by:

$$\rho_{\infty}^{N_2} = \frac{\rho_{in}^{N_2} + \rho_{out}^{N_2}}{2} \quad (22)$$

$$\rho_{in}^{N_2} = \frac{\dot{m}_{in}^{N_2}}{\dot{V}_{O_2} + \dot{V}_{N_2}} \quad (23)$$

$$\rho_{out}^{N_2} = \frac{\dot{m}_{in}^{N_2}}{\dot{V}_{N_2} + \dot{V}_{O_2} - \frac{\dot{m}_{in}^{O_2} - \dot{m}_{O_2}}{\rho_{in}^{O_2}}} \quad (24)$$

The mass concentration of nitrogen at the cathode/electrolyte interface is:

$$\rho_{it}^{N_2} = \left( \frac{\dot{m}_{in}^{N_2}}{\dot{V}_{O_2} + \dot{V}_{N_2}} + \frac{\dot{m}_{in}^{N_2} - \frac{I}{4F} M_{O_2}}{\dot{V}_{N_2} + \dot{V}_{O_2} - \frac{\dot{m}_{in}^{O_2} - \frac{I}{4F} M_{O_2}}{\rho_{in}^{O_2}}} \right) / 2 \quad (25)$$

Now, with the mass concentrations of all species in the air stream available, the partial pressure of oxygen at the cathode/electrolyte interface is determined:

$$p_{it}^{O_2} = \frac{\rho_{it}^{O_2} / M_{O_2}}{\rho_{it}^{O_2} / M_{O_2} + \rho_{it}^{N_2} / M_{N_2}} p_{air} \quad (26)$$

Similar analysis procedures are applicable to hydrogen and water vapor in the fuel stream. The molar flow rate does not change in the fuel stream; therefore, the mass concentration of hydrogen is

$$\rho_{it}^{H_2} = \left( \frac{\dot{m}_{in}^{H_2}}{\dot{V}} + \frac{\dot{m}_{in}^{H_2} - \frac{I}{2F} M_{H_2}}{\dot{V}} \right) / 2 - \frac{i}{2FH_{H_2}} M_{H_2} \quad (27)$$

and for water vapor:

$$\rho_{it}^{H_2O} = \left( \frac{\dot{m}_{in}^{H_2O}}{\dot{V}} + \frac{\dot{m}_{in}^{H_2O} + \frac{I}{2F} M_{H_2O}}{\dot{V}} \right) / 2 + \frac{I}{2FAH_{H_2O}} M_{H_2O} \quad (28)$$

Finally the partial pressures of hydrogen and water are

$$p_{it}^{H_2} = \frac{\rho_{it}^{H_2} / M_{H_2}}{\rho_{it}^{H_2} / M_{H_2} + \rho_{it}^{H_2O} / M_{H_2O}} p_{fuel} \quad (29)$$

$$p_{it}^{H_2O} = \frac{\rho_{it}^{H_2O} / M_{H_2O}}{\rho_{it}^{H_2} / M_{H_2} + \rho_{it}^{H_2O} / M_{H_2O}} p_{fuel} \quad (30)$$

Gas species in a solid oxide fuel cell have high temperatures and low pressures, making ideal gas assumptions plausible when calculating the volume flow rates in many of the above equations. A unit area of  $A$  ( $m^2$ ) for the mass transfer surface or area of electrolyte layer is used in the above equations. The total current and the mass flow rate at the inlet for the fuel cell are determined based on the unit area and the current density of interest, as well as the fuel and oxygen utilization coefficients. However, after operation of equations, partial pressures are consequently independent of the area of mass transfer or electrolyte layer used in the analysis. It is assumed that the electrical current due to electrochemical

reaction comes only from the area of  $D_0 - D_c$ , shown in Fig.3. There may be a small amount of gas diffusing to underneath the current collectors, but it is in the lateral direction and is negligible. Consequently, it is considered that the current collector of size  $D_c$  controls the area of size  $D_0$ . An electrochemical reaction occurs at the area  $D_0 - D_c$  and a current is thus collected laterally and conducts out through the current collectors.

### 3. Properties and conditions in the analysis

Prescribed conditions for analytical computation should include the fuel cell voltage, temperature, and stoichiometric coefficients of fuel and oxygen/air. The components dimensions and properties of the SOFC analyzed in this work are given in Tables 1 and 2. The mass transfer coefficient in Eq. (6) is obtained based on an assumption of laminar flow with a Sherwood number of 3.66 and a characteristic length of 3mm for both the channels with 2D ribs and 3D pillars. This assumption allows the comparison of the fuel cell performance with flow fields using 2D ribs and 3D pillars on a common basis. A contact resistance of  $5.0 \times 10^{-3} \Omega \text{ cm}^2$  between a current collector and an electrode is used. Hydrogen fuel with a stoichiometric coefficient of 1.2 and air at the oxygen stoichiometric coefficient of 2.0 are considered. The operating temperature of the fuel cells is  $800^\circ\text{C}$ . SOFCs with functional graded electrode/electrolyte layers are considered, and thus the exchange current densities for activation polarization are  $12000 \text{ A/m}^2$  and  $24000 \text{ A/m}^2$  on the cathode and anode, respectively.

Table 1. Component thicknesses and porosities

	Components	Thickness	Porosity
Cathode Current Collecting Layer (CCCL)	LSCF	$60 \mu\text{m}$	0.32
Cathode Functional Layer (CFL)	LSCF/S <sub>10</sub> SZ	$30 \mu\text{m}$	0.40
Electrolyte Layer (EL)	S <sub>10</sub> SZ	$10 \mu\text{m}$	< 0.03
Anode Functional Layer (AFL)	Ni/S <sub>10</sub> SZ	$20 \mu\text{m}$	0.10
Anode Support (AS)	Ni/S <sub>10</sub> SZ	$1000 \mu\text{m}$	0.55

## 4. Results and discussions

The computation based on the analytical model will study and compare the maximum power densities from SOFCs using 2D ribs and 3D pillars as current collectors.

### 4.1. Spacing and dimensions of 2D ribs

The investigation of the power densities versus current collector size in the SOFC took a fixed control area  $D_0$ . At various  $D_c$ , the power densities are obtained. Shown in Fig.5 are the power densities when a fixed  $D_0$  is 2mm and  $D_c$  changes from 0.4mm to 1.5mm. Apparently, when a current collector takes a large portion of the fixed area, less space is left for reaction, causing a low maximum power density. Reducing the current collector from 1.5mm to 0.6mm increases the maximum power density as seen in Fig.5. On the other hand, when the current collector is smaller than  $D_c=0.6\text{mm}$ , the ohmic loss becomes overwhelming and the maximum power density drops again. In Fig.6,  $D_0$  is 3mm and  $D_c$  changes from 0.7mm to 1.8mm. A similar relationship between the current collector size and the maximum power density is obtained. An optimum size for the current collector is found in both cases. For  $D_0=2\text{mm}$ , the best  $D_c$  is 0.6mm, giving a maximum power density of  $1.77\text{W/cm}^2$ . For  $D_0=3\text{mm}$ , the best  $D_c$  is 1.0mm, giving a maximum power density of  $1.70 \text{ W/cm}^2$ . It is important to know from the above results that there is an optimum size for the current collector in each case, both having fixed control areas. Further observation indicates that a smaller control area allows for greater maximum power density, although there is no doubt that fabrication technology will be the limiting factor.

Table 2. Materials and conductivity

Component	Material	Conductivity at $800^\circ\text{C}$ $\sigma$ (S/cm)
(CCCL)	LSCF	380
(CFL)	LSCF/S <sub>10</sub> SZ	130
(EL)	S <sub>10</sub> SZ	0.090
(AFL)	Ni/S <sub>10</sub> SZ	1100
(AS)	Ni/S <sub>10</sub> SZ	1400

(For porous media, conductivity  $\sigma_{\text{eff}} = \sigma(1 - \varepsilon)^{-1.5}$  [18, 19])

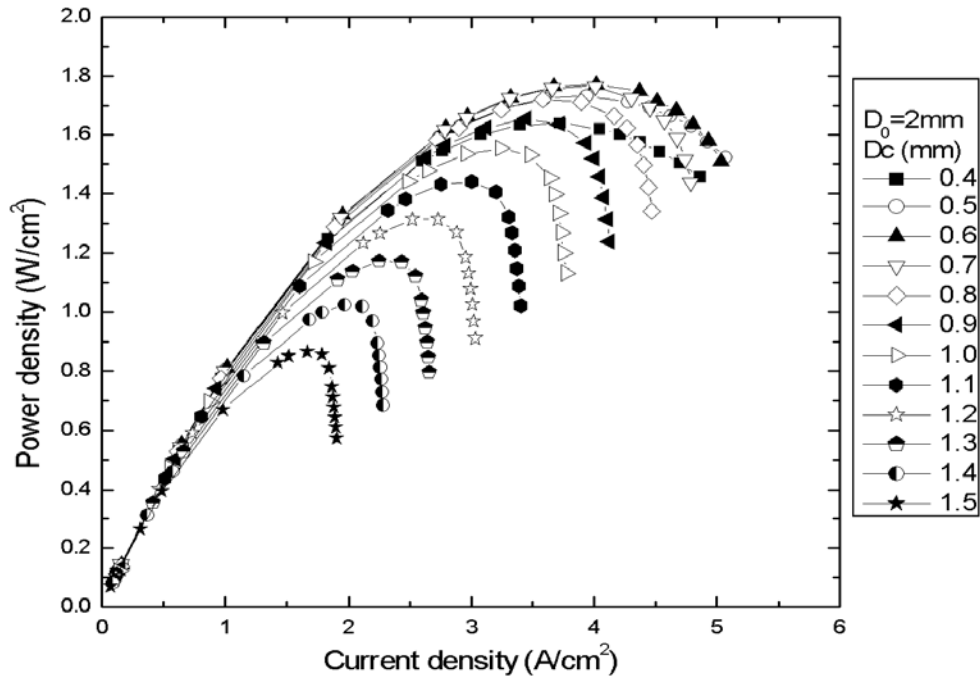


Fig. 5: Power densities at D<sub>0</sub>=2mm and various D<sub>c</sub> for 2D ribs

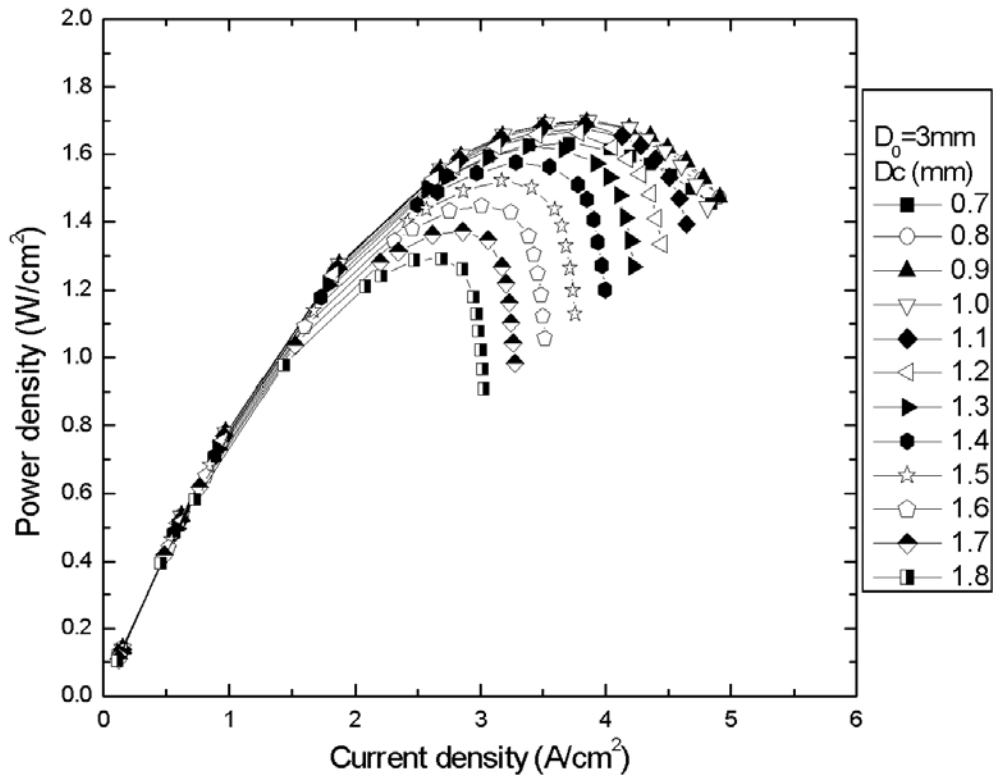


Fig. 6: Power densities at D<sub>0</sub>=3mm and various D<sub>c</sub> for 2D ribs

#### 4.2. Optimization of the spacing and dimension of 3D pillars

Similar investigation of the power densities versus current collector size was conducted for 3D pillars as current collectors. Again, two cases of fixed control area in diameter of  $D_0=2\text{mm}$  and  $D_0=3\text{mm}$  were selected. At various current collector diameters  $D_c$ , the power densities were obtained. Shown in Fig.7 are the power densities when a fixed diameter is  $D_0=2\text{mm}$ , and  $D_c$  changes from 0.4mm to 1.5mm. The optimal diameter  $D_c$  is 1.1mm, at which the maximum power density is  $1.80\text{ W/cm}^2$ , 1.7% higher than the case of a 2D rib. In Fig.8, the diameter of the control area is  $D_0=3\text{mm}$ , and  $D_c$  ranges from 0.9mm to 2.1mm. The optimal diameter of the current collector is  $D_c=1.6\text{mm}$ , which obtains a maximum power density of  $1.75\text{ W/cm}^2$ . This is 2.9% higher than that in the case of a 2D rib.

Again, a similar phenomenon for the 3D pillar current collectors is observed in that a smaller control area makes greater power densities available. This trend of maximum power densities and optimal size of current collectors is obviously independent of the geometrical shape of the current collectors. It is very interesting to see the difference of the maximum power densities between the use of 2D ribs and 3D pillars as current collectors. About 2-3% greater power densities may be available if 3D pillars replace 2D ribs.

To elucidate the phenomenon of the better performance of the 3D pillars, two points are examined. Firstly, for the optimum current collectors of both 2D and 3D cases, it is interesting to find that the ratio of the area of active electrochemical reaction to the total control area is nearly the same. For example, it is about 70% when  $D_0=2\text{mm}$  and 67% when  $D_0=3\text{mm}$ . However, the length of the current collecting route in the 2D case is longer. When  $D_0=2\text{mm}$ , the optimum case has  $(D_0-D_c)/2=0.7\text{mm}$  for 2D ribs and  $(D_0-D_c)/2=0.45\text{mm}$  for 3D pillars; when  $D_0=3\text{mm}$ , the optimum case has  $(D_0-D_c)/2=1.0\text{mm}$  for 2D ribs and  $(D_0-D_c)/2=0.6\text{mm}$  for 3D pillars. Apparently the shorter current collection route in the case of 3D pillars is favorable for the reduction of ohmic loss.

The above comparison of the area ratio and the length of the current collection route can also

explain why a greater power density is obtained in the case of a smaller current collection area. For the cases of  $D_0=2\text{mm}$ , there is a larger area ratio for the active electrochemical reaction and the current collection route is shorter compared to that of cases of  $D_0=3\text{mm}$ . Since this trend exists for both 2D ribs and 3D pillars, a greater power density is always obtained in the case of a smaller current collection area. Nevertheless, it is worth noting to designers of bipolar plates of SOFCs that all the above discussed phenomena are for the optimized current collectors. Due to improvement of flow mixing, 3D current collectors may be highly recommended for the improvement of fuel cell power densities. Of course, this depends on whether a uniform flow distribution to the field is available, as has been achieved in the author's group.

#### 5. Conclusions

This paper presents an analytical model and analysis for the power densities in SOFCs when current collectors of different geometries and size are used. The analysis made clear that there are optimal size and spacing of current collectors for both types of current collectors and flow fields. It is recommended that 3D pillars be used for current collectors in SOFCs with appropriate measures taken for a uniform flow distribution. Unless limited by the fabrication technologies for the bipolar plates, a smaller control area and optimized current collectors can aide in achieving higher power densities in SOFC systems.

#### 6. Nomenclature

$A$	Reaction area ( $\text{m}^2$ )
$D$	Diffusivity ( $\text{m/s}$ )
$d_o, D_o$	Distance or diameter of a control area by one current collector ( $\text{m}$ )
$d_c, D_c$	Width or diameter of a current collector ( $\text{m}$ )
$\bar{E}$	Electromotive force in the modeling circuit ( $\text{V}$ )
$E^o$	Electromotive force at standard state ( $\text{V}$ )

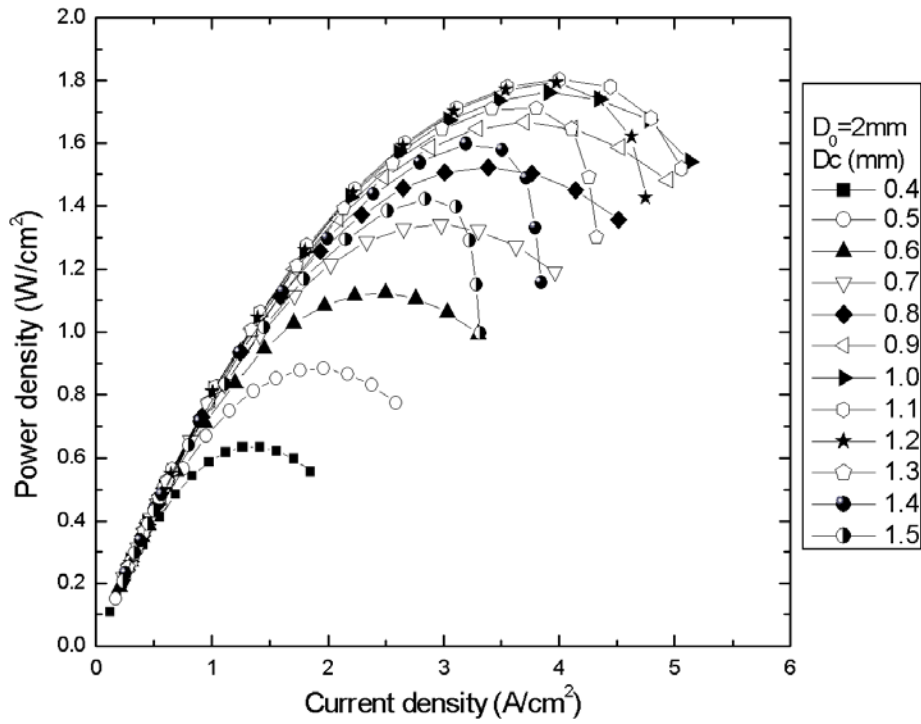


Fig. 7: Power densities at D<sub>0</sub>=2mm and various D<sub>c</sub> for 3D ribs

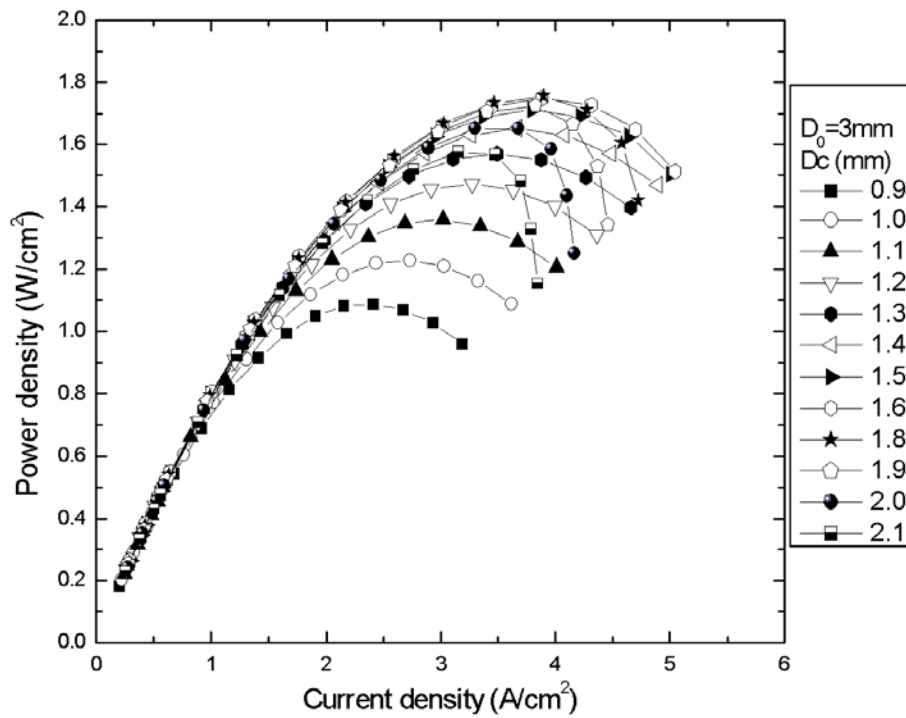


Fig. 8: Power densities at D<sub>0</sub>=3mm and various D<sub>c</sub> for 3D ribs



- anode-supported SOFCs, *Journal of Power Sources* 141 (2005) 216-226.
- [7] Wei Guo Wang, Mogens Mogensen, High-performance lanthanum-ferrite-based cathode for SOFC, *Solid State Ionics* 176 (2005) 457-462.
- [8] N.T. Hart, N.P. Brandon, M.J. Day, N. Lapena-Rey, Functionally graded composite cathodes for solid oxide fuel cells, *J. Power Sources* 106 (2002) 42-50.
- [9] H.Y. Jung, W.-S. Kim, S.-H. Choi, H.-C. Kim, J. Kim, H.-W. Lee, J.-H. Lee, Effect of cathode current-collecting layer on unit-cell performance of anode-supported solid oxide fuel cells, *J. Power Sources* 155 (2006) 145-151.
- [10] Xingyan Xu, Changrong Xia, Guoliang Xiao and Dingkun Peng, Fabrication and performance of functionally graded cathodes for IT-SOFCs based on doped ceria electrolytes, *Solid State Ionics* 176 (2005) 1513-1520.
- [11] F. Zhao, and A. V. Virkar, Dependence of polarization in anode-supported solid oxide fuel cells on various cell parameters, *J. Power Sources* 141 (2005) 79-95.
- [12] Xianguo Li, *Principles of Fuel Cells*, ISBN 1-59169-022-6, Taylor & Francis, New York, 2006.
- [13] C. A. Reiser and R. D. Sawyer, Solid polymer electrolyte fuel cell stack water management system, 1988, US Patent 4,769,297.
- [14] C. A. Reiser, Water and heat management in solid polymer fuel cell stack, 1989, U.S. Patent 4,826,742.
- [15] J. H. Whiton, Y. Wang, C. A. Reiser, G.S. Hirko JR., Small volume fuel cell inlet fuel gas distribution having low pressure drop, 2006, U.S. Patent 20060280995A.
- [16] D. P. Wilkinson, G. J. Lamont, H. H. Voss, C. Schwab, Embossed fluid flow field plate for electrochemical fuel cells, 1996, US Patent, 5,521,018.
- [17] P. W. Li, Uniform Flow Distributor/Collector, 2007, Provisional patent case UA07-093, The University of Arizona.
- [18] James N. Roberts and Lawrence M. Schwartz, Grain consolidation and electrical conductivity in porous media, *Physical review B* 31 (1985) 5990-5998.

M. A. Ioannidis, M. J. Kwiecien, I. Chatzis, Electrical conductivity and percolation aspects of statistically homogeneous porous media, *J. Transport in Porous Media* 29 (1997) 61-83.

## Biographies



**Peiwen Li** earned his Ph.D. (1995) degrees in energy and power engineering area from Xi'an Jiaotong University, China. He is currently an assistant professor in the Department of Aerospace and Mechanical Engineering at the University of Arizona, USA. He has been interested in heat transfer enhancement in industrial processes, turbulence drag reduction, gas turbine cooling technologies, the multi-physics transport phenomena in fuel cells and electrolysis cells, and concentrated solar thermal power systems. Professor Li is an active member of the American Society of Mechanical Engineers. He is also a reviewer of papers for more than 10 technical Journals.



**Gege Tao** received his Ph. D. from the Department of Aerospace and Mechanical Engineering at the University of Arizona in 2003, USA. Dr. Gege Tao is a senior Research Scientist at the Materials and Systems Research Inc. (MSRI), Salt Lake City, Utah, USA. His research interests focus on the electrochemical devices R&D for renewable energy storage & power generation applications, including the reversible solid oxide fuel cells/electrolyzers and batteries.



**Hong Liu** received her Bachelor degree (2005) in energy and power engineering area from Xi'an Jiaotong University, China. She is currently a Ph.D. student in the Department of Aerospace and Mechanical Engineering at the University of Arizona, USA. Her research focuses on numerical analysis of fluid flow and heat transfer in industrial processes, energy systems. Her Ph.D. dissertation work is experimental and numerical study of the multi-physics transport phenomena in internal reforming solid oxide fuel cells.